Actinic fluxes in Titan's atmosphere, from one to three dimensions: Application to high-latitude composition

Sébastien Lebonnois and Dominique Toublanc

Centre d'Etude Spatiale des Rayonnements, Toulouse, France

Abstract. We present a study on diurnally and annually averaged values of the actinic fluxes used in one-dimensional (1-D) photochemical models, as well as a 3-D radiative transfer model, based on Monte Carlo calculations with application to the atmosphere of Titan. This study shows that the commonly used value $< \theta >= 30°$ for the mean incident angle at the equator in photochemical models of Titan is not the best choice, though changing the value has no dramatic effects on photochemistry. The results of the 3-D code give direct access to the photolysis rates at any point in the atmosphere. The necessity of 3-D values in a deep atmosphere such as Titan's is demonstrated particularly for high-latitude winter conditions. These 3-D photolysis rates are used to model the latitudinal variations of the chemical composition of Titan's atmosphere in a 1-D photochemical model adapted to different latitudes. This study shows that these kinds of simple photochemical models cannot reproduce the observed latitudinal behavior and that we need to develop real 2-D photochemical models of Titan's atmosphere.

1. Introduction

In the atmosphere of Titan, photochemistry of the major constituents N_2 (98%) and CH_4 (2%) yields a complex hydrocarbon and nitrile chemistry. The wavelengths of interest are in the ultraviolet, from ~10 nm to ~300 nm, including the photochemistry of heavier compounds issued from this chemistry. The composition of Titan has been observed in the infrared by the infrared interferometer spectrometer (IRIS) on board Voyager I, and the data have recently been reanalyzed by *Coustenis et al.* [1989] and *Coustenis and Bézard* [1995]. They obtained the molar fractions of minor conponents of the atmosphere around 100-130 km of altitude, which is in the low stratosphere, for different latitudes. These observations show an enhancement of the mole fraction of some species at high northern latitudes in regions just coming out of winter at the time of Voyager flyby. *Yung* [1987] suggested that a mechanism to explain this enhancement could be the production of these species at high altitudes and diffusion to low atmospheric levels, where no photolysis was present. To explore this possibility, it is necessary to have a closer look at the UV radiation field in the atmosphere. This is the main goal of this paper.

The solar flux used in calculating photodissociation rates is the actinic flux. This is the mean intensity at a given point in the atmosphere, which is different from the net vertical flux used for calculations of radiative heating [*Michelangeli et al.*, 1992]. This actinic flux is computed with the radiative transfer Monte Carlo code developed by *Toublanc et al.* [1995] and *Toublanc* [1996], modified to use fractal aerosol cross sections [*Rannou et al.*, 1995]. This technique makes no distinction between direct and scattered light, although it allows a precise calculation of the scattered light.

For photochemical models of planetary atmospheres it is important to have diurnally averaged values of the solar flux received at each level for a given latitude, either at a given season or averaged over the year. A method of approximation to get the diurnally averaged values of the photolysis coefficients has been developed by *Cogley and Borucki* [1976]. This approximation enables one to use a mean zenith angle to compute actinic fluxes. We computed diurnally averaged actinic fluxes and compared them with the results of this approximation. This comparison confirmed the suitability of Cogley and Borucki's approximation in the case of Titan. We also computed annually averaged actinic fluxes at the equator and used them to identify the best mean incident angle for one-dimensional (1-D) approximation: we obtained $< \theta >= 50°$, which is in disagreement with the annually averaged value of the incident angle at equator commonly used in photochemical models of Titan, $< \theta >= 30°$ [*Yung et al.*, 1984; *Toublanc et al.*, 1995; *Lara et al.*, 1996]. Nevertheless, when the

depth of the atmosphere is comparable to the planet's radius (i.e., Titan's case), a 3-D representation of the solar flux at a particular point in the atmosphere may be more realistic. Therefore a 3-D radiative transfer Monte Carlo code has been developed on the same basis as the 1-D code [*Toublanc et al.*, 1995; *Toublanc*, 1996] and is described in section 3, together with its results for Titan's atmosphere. Comparison between the 3-D latitudinal diurnally averaged photolysis coefficients and the 1-D photolysis coefficients obtained with the previously discussed averages is presented, and as expected for a deep atmosphere, 1-D radiative transfer appears to be a poor approximation for high-latitude winter conditions. To explore *Yung*'s [1987] suggestion, we used the 3-D photolysis coefficients in a 1-D photochemical model adapted to different latitudes and taking into account the seasonal cycle. The results are presented in section 5 and show that vertical diffusion is not enough to explain the expected enrichment, despite the improvement in the description of the UV field.

2. Averaging 1-D Photolysis Rates

2.1. Actinic Fluxes

The Monte Carlo code used is described in detail by *Toublanc et al.* [1995] and *Toublanc* [1996]. The composition of the atmosphere used has been obtained with our 1-D photochemical model [*Toublanc et al.*, 1995]. The cross sections and other data needed are the same as given by *Toublanc et al.* [1995]. The enhancement factor, which will be used in this paper to discuss the actinic fluxes, is defined as follows:

$$f(\lambda, z, \theta) = \frac{F(\lambda, z, \theta)}{F_S(\lambda)} \tag{1}$$

where $F(\lambda, z, \theta)$ is the actinic flux at level z, $F_S(\lambda)$ is the incident flux, i.e., the solar flux received at Saturn's orbit for the wavelength λ, and θ is the incident zenith angle. This factor is obtained directly through the radiative transfer Monte Carlo code.

For a given point at the top of a planetary atmosphere, θ is a function of the solar hour angle h and of the latitude ϕ:

$$\cos\theta(h, \phi, \delta) = \sin\phi \sin\delta + \cos\phi \cos\delta \cos h \tag{2}$$

for $h \in [-H/2, +H/2]$, where δ is the solar declination and H is the radian day length given by

$$\cos\frac{H}{2} = -\tan\phi \tan\delta. \tag{3}$$

The photolysis coefficient (in s^{-1}) of a species is then

$$J = \sum_{\lambda} \sigma(\lambda) f(\lambda) F_S(\lambda), \tag{4}$$

where σ is the absorption cross section for this species.

2.2. Diurnal Average: Mean Zenith Angle

In this section we are interested by the diurnally averaged actinic flux at a given latitude and for a given season. It can be obtained either by integration or by using a mean solar zenith angle $\overline{\theta}(\phi, \delta)$.

To get this angle, $\cos\theta$ is averaged over the sunlit portion of the day:

$$\cos\overline{\theta}(\phi, \delta) = \frac{1}{H} \int_{-\frac{H}{2}}^{\frac{H}{2}} \cos\theta(h, \phi, \delta)\, dh, \tag{5}$$

which gives

$$\cos\overline{\theta}(\phi, \delta) = \sin\phi \sin\delta + \frac{2}{H} \cos\phi \cos\delta \sin\left(\frac{H}{2}\right). \tag{6}$$

This approximation has been tested in previous studies [*Cogley and Borucki*, 1976], and those authors recommend it for wavelengths with small optical depths. We studied the validity of this approximation in the case of Titan, for use in photochemistry, by comparing

$$\overline{f}(\lambda, \phi, \delta) = \frac{H(\phi, \delta)}{2\pi} f[\lambda, \overline{\theta}(\phi, \delta)] \tag{7}$$

with the averaged enhancement factor obtained by integration

$$f_{da}(\lambda, \phi, \delta) = \frac{1}{2\pi} \int_{-\frac{H}{2}}^{+\frac{H}{2}} f[\lambda, \theta(h, \phi, \delta)]\, dh, \tag{8}$$

where da is diurnally averaged. The profiles $f(\lambda, \theta)$ are calculated every 5°, and this integral is then calculated with 2° steps for h.

For all wavelengths the f_{da} profiles are very similar to the ones obtained with the mean incident angle $\overline{f}$ except in certain cases where a slight shift in altitude (~10 km) is observed, but this would not significantly influence photochemical calculations: a shift for the absorption of a few tens of kilometers shifts the production and destruction zones of some species of a few altitude steps, which does not significantly change the composition profiles. In Table 1 we compare integrated photolytic loss rates of CH_4 (calculated with a mean profile) for different situations using f_{da} and $\overline{f}$. This confirms that in most cases, $\overline{f}$ is a good approximation for f_{da}. We can therefore conclude that this mean incident angle $\overline{\theta}$ can yield the correct diurnally averaged 1-D enhancement factor $\overline{f} = f_{da}$.

2.3. Annual Average

In photochemical models, annual mean photolysis coefficients can be used to avoid seasonal dependence. In Titan's case they are computed with a mean incident angle, and the frequently adopted value for $< \theta >$ at the equator is 30° [*Yung et al.*, 1984; *Toublanc et al.*, 1995; *Lara et al.*, 1996]. To look for the best mean incident angle, we computed the annually averaged enhancement factor for the equator f_{aa} as follows:

Table 1. Integrated Loss Rates for the CH_4 Photodissociation in Different Conditions Comparing f_{da} and $\overline{f}$ and f_{aa} and $< f >$ (Different Values of $< \theta >$) for One Dimension and Also 1-D to 3-D Values

	f_{da} (1-D)		$\overline{f}$ (1-D)		$\overline{f}$ (3-D)
Equator, winter	2.02×10^9		2.03×10^9		2.15×10^9
55°N, winter	5.60×10^8		6.00×10^8		8.11×10^8
70°N, winter	0.00		0.00		5.92×10^8
55°N, spring	1.66×10^9		1.85×10^9		1.96×10^9
30°N, summer	2.45×10^9		2.42×10^9		2.56×10^9
70°N, summer	2.46×10^9		2.43×10^9		2.61×10^9
	f_{aa} (1-D)		$< f >$ (1-D)		$< f >$ (3-D)
		$< \theta >= 50°$	$< \theta >= 55°$	$< \theta >= 60°$	
Equator, annual mean	2.10×10^9	2.26×10^9	2.02×10^9	1.79×10^9	2.27×10^9

Units are cm^{-2} s^{-1}. The integrated loss rates were calculated with a mean CH_4 profile.

$$f_{aa}(\lambda) = \frac{1}{2\pi}\int_0^{2\pi} f_{da}(\lambda, 0, \delta)\, dL_s, \tag{9}$$

where L_s is the solar longitude, with

$$\sin\delta = \sin L_s \sin\epsilon, \tag{10}$$

where ϵ is the planet obliquity.

Then we compare f_{aa} with

$$< f > (\lambda) = \frac{H}{2\pi} f(\lambda, < \theta >) = \frac{1}{2} f(\lambda, < \theta >) \tag{11}$$

for different values of $< \theta >$ (Figure 1). It seems that no mean incident angle $< \theta >$ can really reproduce the profile of f_{aa}, but an angle between 50° and 60° may be a correct approximation. Nevertheless, since the profiles slightly differ in altitude by a maximum of 40 km, the exact value of $< \theta >$ may have only few consequences on photochemistry. We also compare in Table 1 the integrated photolysis loss rate of CH_4 for f_{aa} and $< f >$ (obtained for different values of $< \theta >$). Also shown is the loss rate obtained with the 3-D profile for $< f >$ (see sections 3 and 4). From these comparisons we conclude that 50° is the best approximation.

However, at any level, these mean values only take into account solar flux for $h \in [-H/2, +H/2]$, i.e., on the dayside of the terminator plane. For a planet like Titan the appreciable depth of the atmosphere compared to the planet's radius make this hypothesis a poor approximation, and it was necessary to develop a 3-D code to get a more realistic description of the actinic flux at any point in the atmosphere.

3. 3-D Radiative Transfer Code

This 3-D code has been developed on the same basis as the 1-D code. The space referential (OX, OY, OZ) is taken as follows (see Figure 2): O is Titan's center, OZ is the Titan-Sun axis, and (OX, OZ) is the plane containing the rotation axis. A point M in the atmosphere is located by (R, α, β), where R is the distance from M to O, α is the angle in the plane (OX, OY), ranging from $-\pi$ (OX') to π, and β is the angle in the plane (OX, OZ), ranging from $-\pi/2$ (OZ') to $+\pi/2$ (OZ); $\beta = +\pi/2$ is then the subsolar point. The atmosphere is divided into half cones for β values taken with $\Delta\beta = 10°$, half planes for α values also taken with $\Delta\alpha = 10°$, and spheres taken with $\Delta R = 2$ km from $R_P = 2575$ km, Titan's radius, to $R_A = 3875$ km, which is the chosen top of the atmosphere. Because of the symmetry, f depends only on β, so despite the fact that we follow the exact position of the photon in (α, β), integration over α is done to get f.

For each wavelength, from 10 nm to 310 nm (5 nm steps), each element of the sunlit surface ($R = R_A, \beta \in [0, +\pi/2]$, and $\alpha = 0$) received $N = 5\times10^4$ photons, each one representing the destructive energy

$$\delta E_i = \frac{1}{N} F_S(\lambda) \underbrace{(R_A^2 \cos\beta_i\, \Delta\alpha\, \Delta\beta)}_{\text{surface element at position } \beta_i} \sin\beta_i. \tag{12}$$

Those 5×10^4 photons are randomly distributed on the whole surface element and then are individually followed through the atmosphere, step by step (the step length is $\delta s = 0.2$ km). Each time a photon exits a volume element, the actinic flux in this element is increased by

$$\delta F = \frac{\delta E}{R^2 \cos\beta\, \Delta\alpha\, \Delta\beta} \frac{s}{\Delta R}, \tag{13}$$

where s is the total length of the photon's path in this element. We have verified the correct treatment of individual photons by making a test on a transparent, non-scattering atmosphere ($f = 1.$ in all illuminated volume elements).

3.1. Absorption

While the photon goes through the atmosphere, δE is multiplied by $e^{-\tau_{abs}}$, where $\tau_{abs} = \tau_A + \tau_G$ and τ_A and

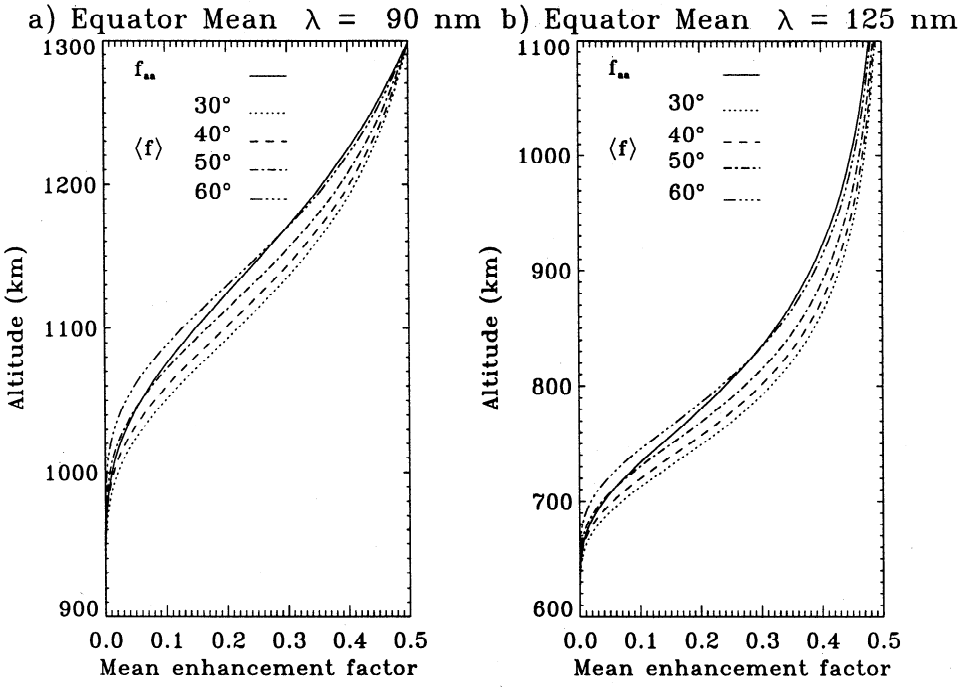

Figure 1. Comparison between enhancement factor f_{aa}^{1-D} and $< f >^{1-D}$ profiles obtained for different values of $< \theta >$ at two chosen wavelengths: (a) $\lambda = 90$ nm within absorption bands of N_2 and (b) $\lambda = 125$ nm with a 5 nm wide channel containing Lyman alpha.

τ_G are the optical depths of absorption by aerosols and gases, respectively. For a path length s in one volume element,

$$\tau_{\text{abs}} = -\frac{s}{\Delta R}\left[\Delta\tau_A + \Delta\left(\int_h \sigma_{\text{abs}}\, n(z)\, dz\right)\right], \quad (14)$$

where Δ refers to the variation between radial distances R and $R + \Delta R$ bounding the volume element, $\sigma_{\text{abs}}(\lambda)$ is the mean gaseous absorption cross section, and $n(z)$ is the number density at level z.

3.2. Scattering

The probability of a photon to be scattered at an optical depth τ is $e^{-\tau}$. The most probable optical depth where the scattering should occur is randomly chosen according to this exponential law: $\tau_{\text{max}} = -\ln(1 - r)$,

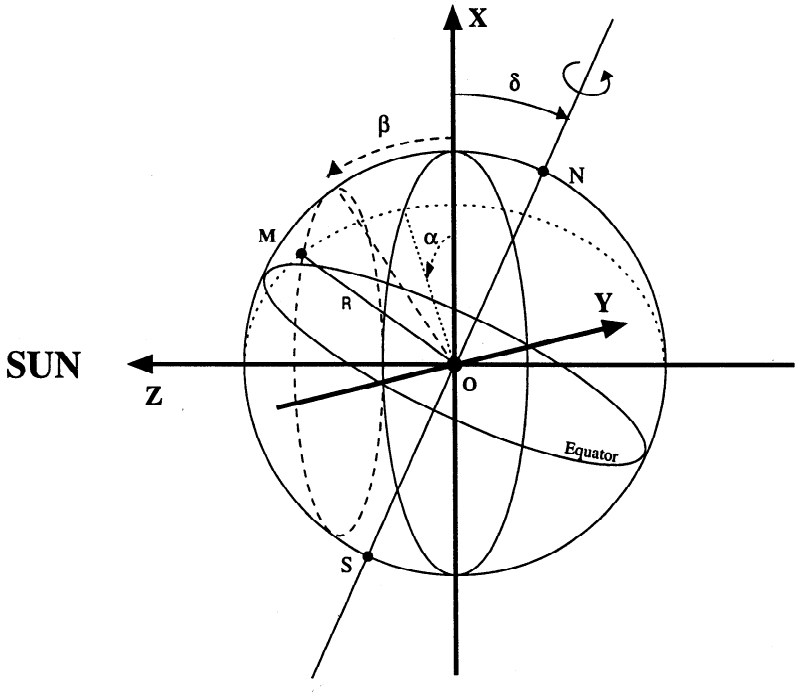

Figure 2. Geometry and notations used in the three-dimensional (3-D) Monte Carlo code.

where r is a random number $r \in [0,1]$. The opacity $\tau_{\rm scat}$ is put to zero after each scattering and increased at each photon step by

$$\delta\tau_{\rm scat} = \frac{\delta s}{\Delta R}\left[\Delta\tau_F + \Delta\left(\int_h \sigma_R\, n_{\rm N_2}(z)\, dz\right)\right], \quad (15)$$

where σ_R is the cross section for Rayleigh scattering mainly by N_2 and τ_F is the optical depth of aerosols for fractal scattering

$$\tau_F = \int_h \sigma_F\, n_A(z)\, dz, \quad (16)$$

where σ_F is the scattering cross section for fractal aerosol particules and $n_A(z)$ is the particule density at level z. When $\tau_{\rm scat} \geq \tau_{\rm max}$, a scattering event occurs, and we randomly choose between Rayleigh or fractal aerosols scattering: $f_R = \tau_R/(\tau_R + \tau_F)$; if $r \in [0, f_R]$, a Rayleigh scattering occurs, otherwise a fractal aerosols scattering occurs. The new direction for the photon is then computed.

When a photon reaches the top of the atmosphere ($R \geq R_A$), it escapes, and the procedure starts again with the next photon. When it reaches the ground ($R \leq R_P$), we randomly choose if it is scattered or absorbed. The ground albedo was fixed at 0.2 for all wavelengths. When scattered, the new direction is computed with a uniform probability over the solid angles. At the end of the calculations we get, for each volume element, the enhancement factor f.

4. The 3-D Latitudinal Diurnal Averages

A point in the atmosphere located by (R, ϕ, h) can also be located with (R, α, β) by a simple rotation of $((\pi/2) - \delta)$ around the OY axis. Because of the symmetry around the OZ axis, only β is needed to find f:

$$\cos\beta = \cos\phi\cos h\cos\delta + \sin\phi\sin\delta. \quad (17)$$

The diurnal average profile of f can then be evaluated at a given latitude by

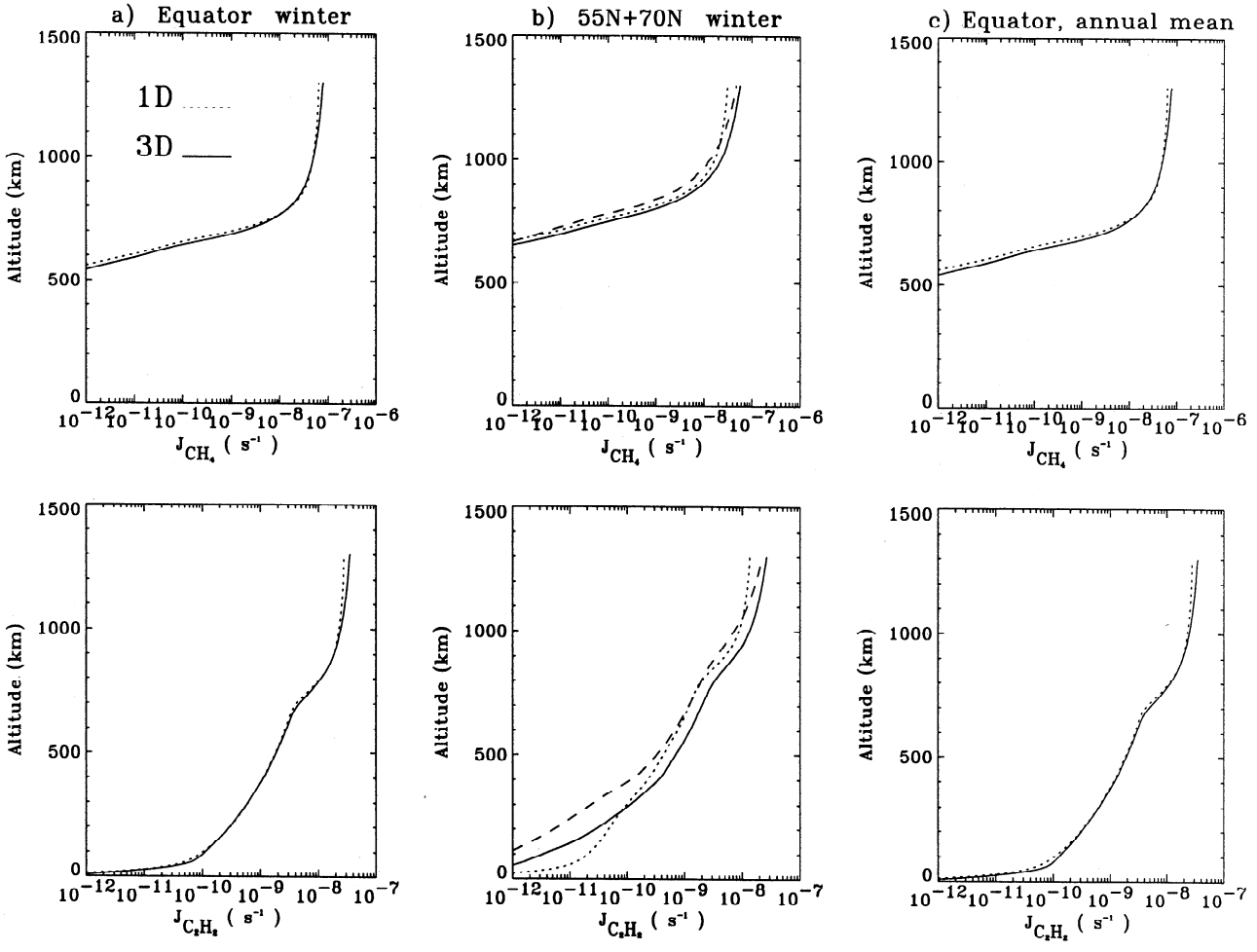

Figure 3. (a and b) Comparison between photodissociation coefficients J^{1-D} (dotted lines) and J^{3-D} (solid lines) for CH_4 and C_2H_2 in winter for three latitudes. In Figure 3b, J^{3-D} for 70°N is shown by a dashed line (for these conditions, $J^{1-D} = 0$). (c) Comparison between J^{3-D} (solid lines) and J^{1-D} (dotted line) (obtained with $< \theta > = 50°$) in the case of the annual average at the equator.

$$\overline{f}(\lambda,\phi,\delta) = \frac{1}{2\pi}\int_0^{2\pi} f(\lambda,\beta)\, dh. \qquad (18)$$

The integral is again computed with 2° steps in h. The annual average profile of f at the equator is also computed with

$$< f >= \frac{1}{2\pi}\int_0^{2\pi} \overline{f}(\delta)\, dL_s. \qquad (19)$$

4.1. Comparison of 1-D and 3-D fluxes

To compare 1-D and 3-D actinic fluxes, photolysis coefficients for CH_4 and C_2H_2 have been computed for different latitudes and seasons from $\overline{f}(\phi,\delta)$ and for the annual average at the equator from $< f >$. The integrated loss rates for $CH_4 + h\nu$ have also been calculated for comparison between 1-D and 3-D fluxes in different conditions and are also presented in Table 1. We can see in this comparison that the difference between 1-D and 3-D rates is less than or around 10% in most conditions, except for high latitudes in winter.

In Figure 3 we present these photodissociation coefficients in winter for three latitudes and for the annual mean at the equator. To enhance the differences between 3-D and 1-D fluxes, we plot in Figure 4 the "contrast" $\alpha(\phi,z)$ for C_2H_2:

$$\alpha(\phi,z) = 2\frac{J^{3-D}(\phi,z) - J^{1-D}(\phi,z)}{J^{3-D}(\phi,z) + J^{1-D}(\phi,z)}. \qquad (20)$$

The medium shaded zone ($\alpha \in [-0.2, 0.2]$) indicates a difference between 1-D and 3-D photodissociation coefficients <20%. The difference between 1-D and 3-D diurnal averages essentially lies in the actinic fluxes from the night hemisphere. In 1-D models, the sum is made only between $h = -H/2$ and $h = +H/2$, and the nightside contributions are neglected. This restriction explains the high values of α for high-latitude winter conditions and for high altitudes. The importance of using 3-D photodissociation coefficients is obvious for latitudes above the polar circle (63.3°): when $H = 0$ in winter, $J^{1-D} = 0$, but J^{3-D} is of the same order as for latitudes below the polar circle. From Figure 4, it can be seen that 1-D fluxes are also a poor approximation for the low atmosphere ($z < 200$ km). For high latitudes, at altitudes corresponding to the haze layer [see, e.g., *Sagan and Thompson*, 1984], the path length inside the haze may be much higher in the 3-D model than

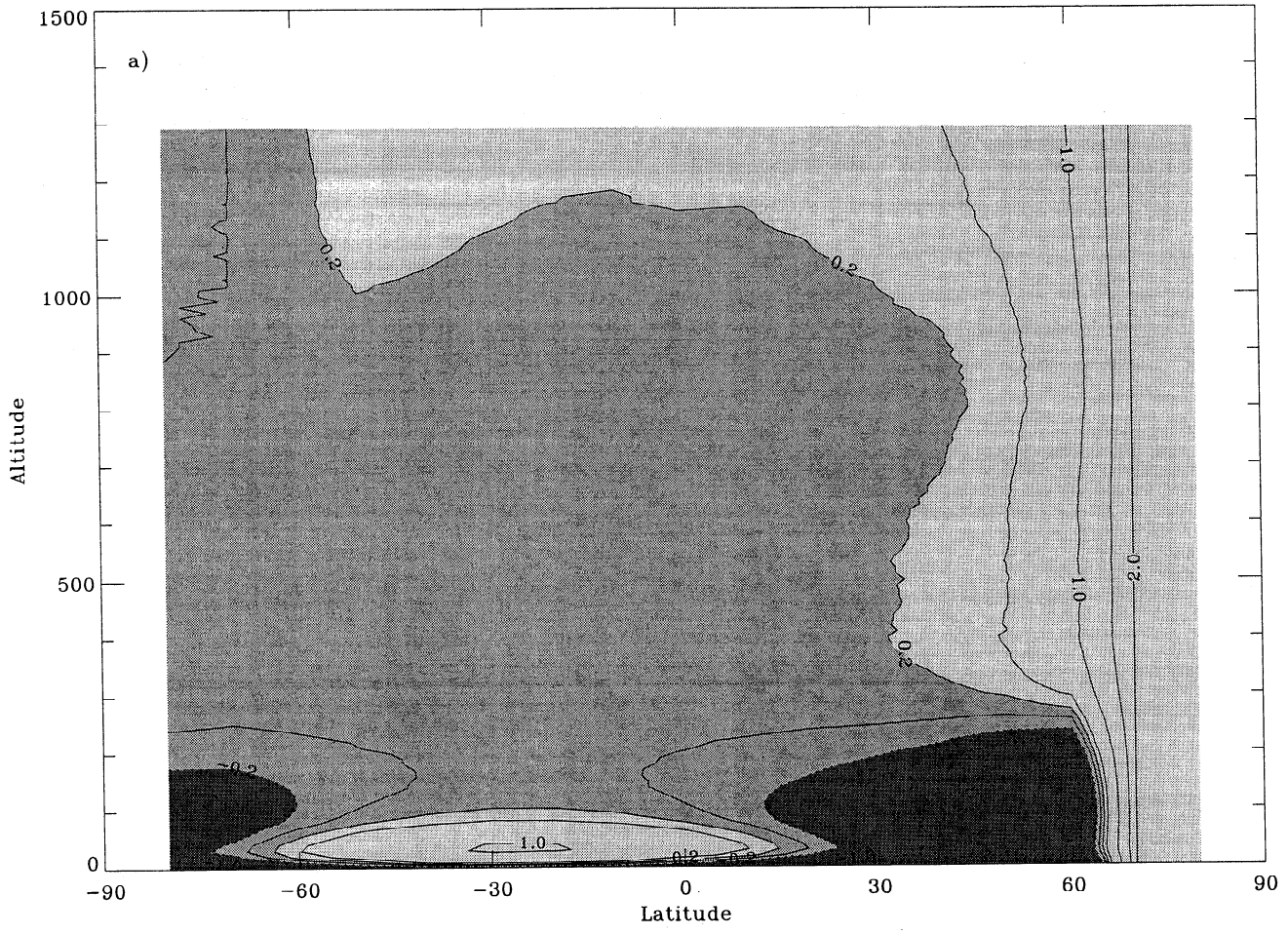

Figure 4. Contrast α (see text for definition) for C_2H_2 (a) at solstice and (b) at equinox. The medium shaded zone ($\alpha \in [-0.2, 0.2]$) indicates a difference between 1-D and 3-D photodissociation coefficients <20%.

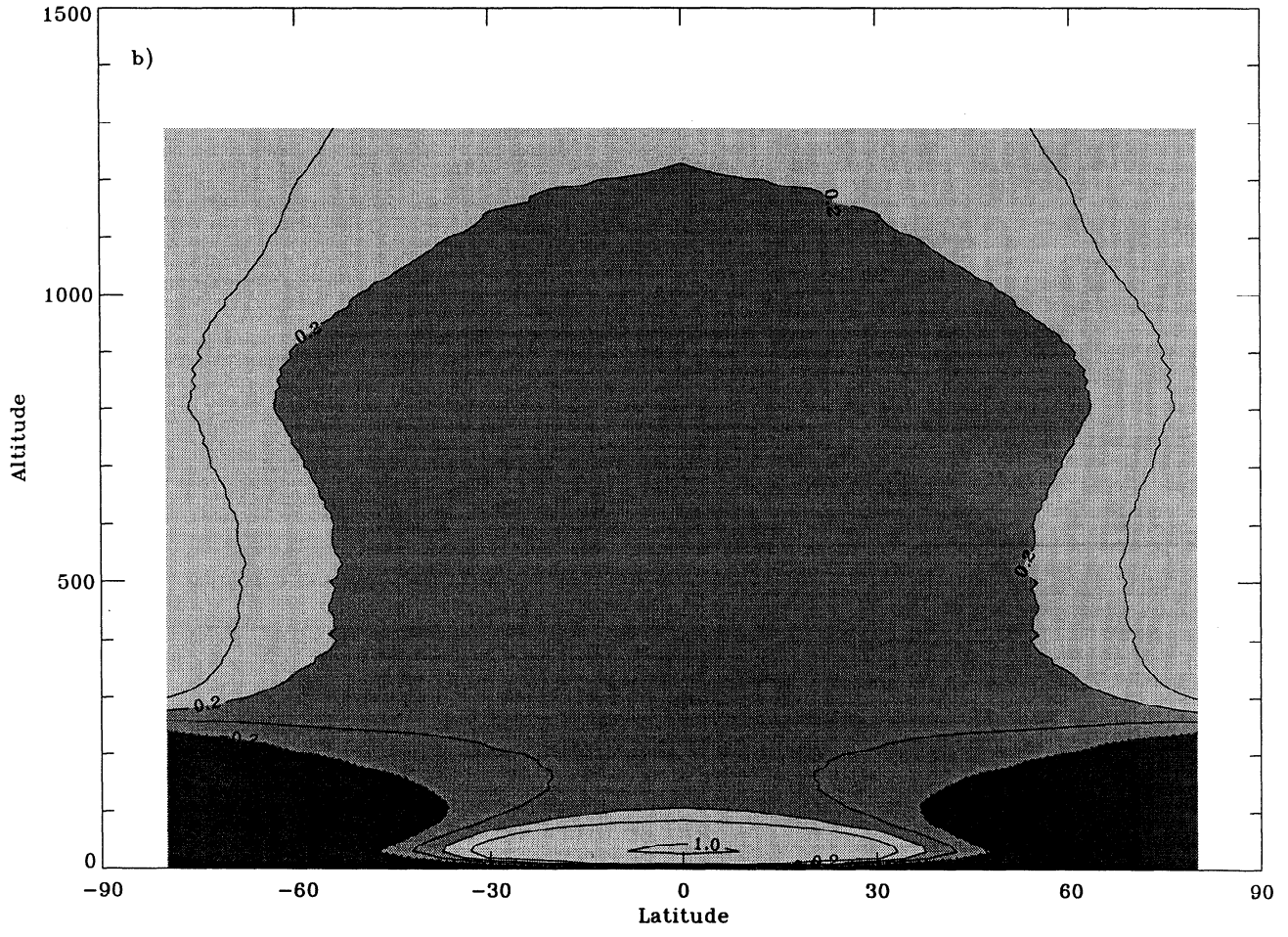

Figure 4. (continued)

simply modeled with the Chapman function [see *Toublanc et al.*, 1995]. This could explain the overestimation of the 1-D flux (Figure 4, dark shaded zones). Near the subsolar point the essential contribution is from the dayside, especially for low altitudes, and the flux coming from the zenith has a strong contribution: its crossing of the haze layer may be badly reproduced by a mean zenith angle and the Chapman function, yielding the underestimation of the 1-D flux (Figure 4, light shaded zone at low altitudes, centered on the subsolar point).

4.2. Discussion of High Latitudes

To investigate the mechanism suggested by *Yung* [1987] to explain the enhancement of nitriles at high latitudes coming out of winter, we computed the photolysis coefficients of HCN (source of CN radicals), HC_3N, and C_2N_2 in winter at equator and 70°. Results are presented in Figure 5. Indeed, there is a differential photolytic behavior between the mesosphere (~300-500 km) and the stratosphere (~70-250 km) as the latitude increases from equator to the winter pole: for stratospheric altitudes the decrease of the photodissociation coefficients at 70° compared to equator is more pronounced than for mesospheric altitudes, but this mesospheric decrease can already be significant. Therefore there may be a relative enrichment for low altitudes at high latitudes compared to the equator, but there may also be less production of nitriles in the mesosphere. Whether this can lead to the observed enrichment in the low stratosphere is not a simple question and requires a 2-D photochemical model to explore the dynamical part of the problem. In section 5, we will show 1-D calculations as a first approach to this problem.

5. The 1-D Photochemical Calculations With Adaptable Latitude

5.1. Model

With a 3-D description of the UV field we were able to develop a pseudo 2-D photochemical model which could follow the seasonal cycle at a chosen latitude: the latitude-altitude plane is divided in columns, with no exchange between them. In each column (the latitude is fixed, from equator to 70°) the photolysis coefficients are evolving with Saturn's revolution around the Sun, and the only transport is vertical eddy diffusion. This model is an updated version based on the model described by *Toublanc et al.* [1995] (the update is essen-

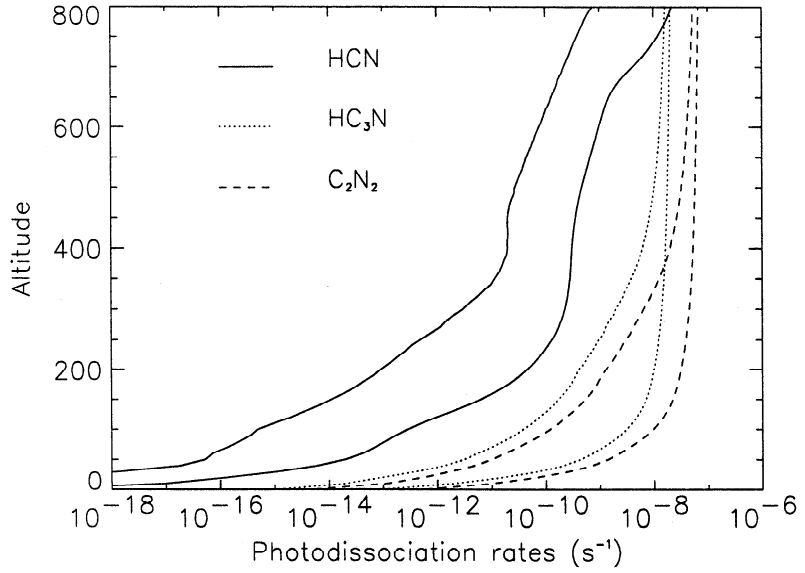

Figure 5. Photodissociation coefficients for HCN, HC_3N and C_2N_2 at winter solstice for two latitudes: 70° (lowest values) and the equator (highest values).

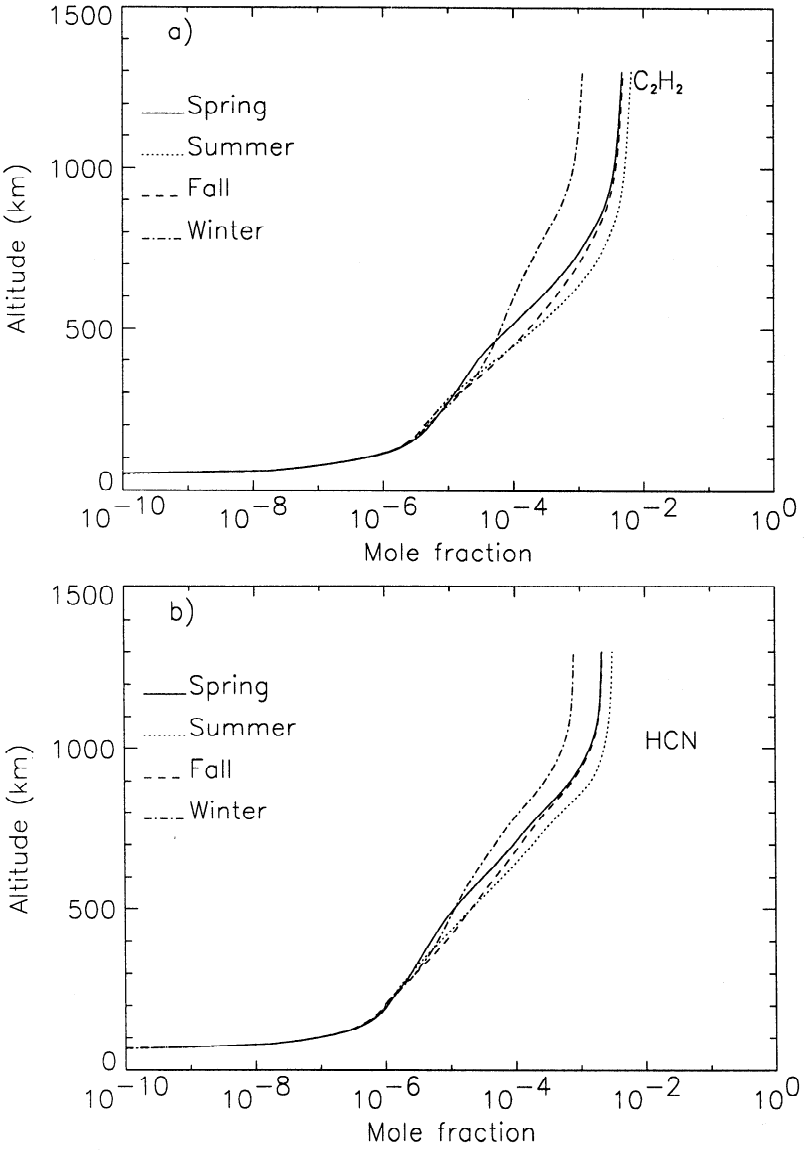

Figure 6. Seasonal behavior of the (a) C_2H_2 and (b) HCN profiles at 70° latitude.

tially based on new reaction rates that have been measured after the publication of this model). The eddy diffusion coefficient profile is also taken from *Toublanc et al.* [1995] and was kept constant with latitude. We used the resulting compositions, as functions of latitude and season, to test Yung's hypothesis.

5.2. Results and Discussion

The seasonal and latitudinal behavior is, in this model, fairly similar for all constituents.

5.2.1. Seasonal oscillations. The oscillations in the photolysis coefficients induce oscillations in the composition of the atmosphere down to the high stratosphere. Below approximately $z = 200$ km the composition at a given latitude is not affected by the seasonal cycle (see Figures 6a and 6b for C_2H_2 and HCN behavior for 70°N). Therefore two symmetric latitudes have, in this model, an identical low stratospheric composition around the year. This contradicts the Voyager observations, where the high latitudes coming out of winter have a clearly different low stratospheric composition from the other hemisphere, which means an asymmetry between spring and fall.

5.2.2. Latitudinal variations at spring equinox. We present in Figure 7 profiles of C_2H_2 and HCN for latitudes from 70°N to 70°S, in the altitude range $z \in [0, 500]$ km. The boxes are the Voyager observations as a function of latitude [*Coustenis et al.*, 1995]. Three points can be drawn from these profiles: (1) These variations are, in the low stratosphere, symmetric with respect to the equator (as it was seen in section 5.2.1). (2) There is a relative enrichment of the low stratosphere for 70°N, coming out of winter. This is coherent with Yung's hypothesis and with the results we discussed in section 4.2. This is the general behavior for most of the constituents in these simulations. (3) This relative enrichment of the low stratosphere (compared to meso-

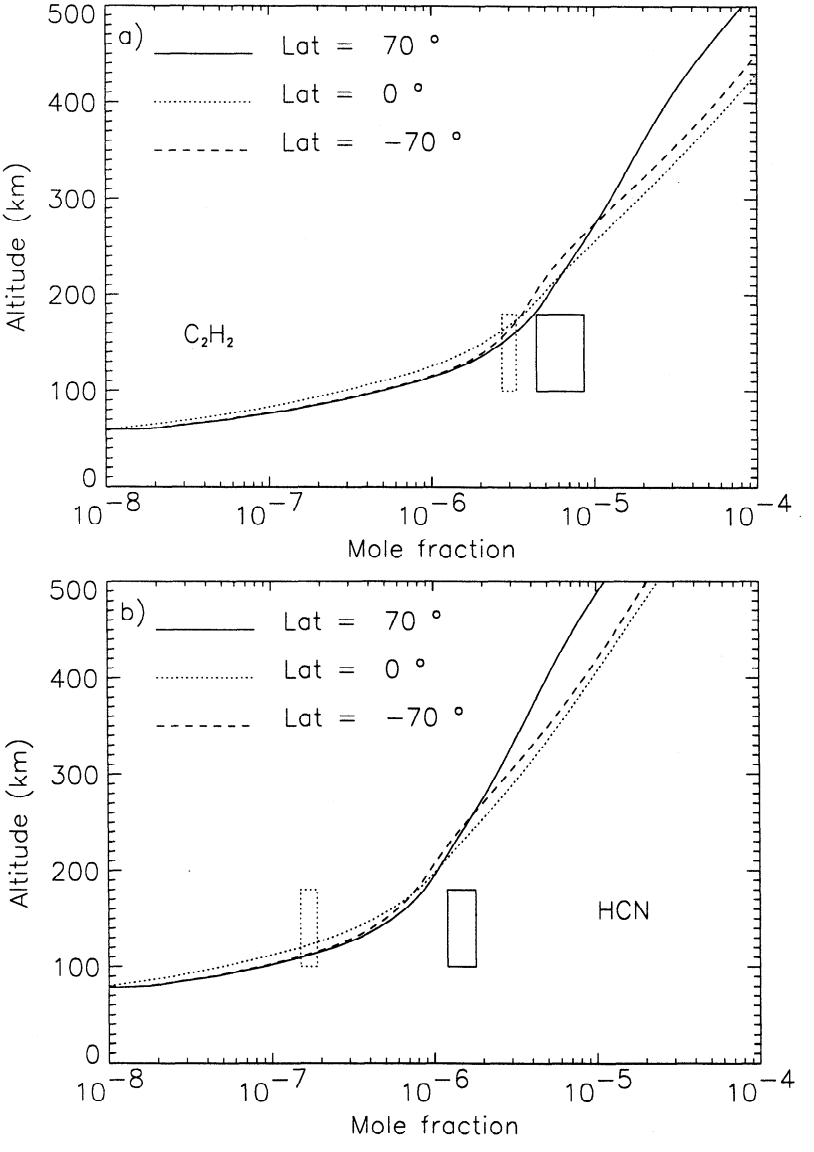

Figure 7. Latitudinal behavior of the (a) C_2H_2 and (b) HCN profiles at northern spring equinox. The boxes are the Voyager observations (for the equator and 70°N) [*Coustenis et al.*, 1995].

sphere) for 70°N yields the stratospheric levels at high latitudes that remain comparable to equatorial stratospheric levels, despite the depletion in the mesosphere. It cannot explain the enhancement observed by Voyager.

Therefore the vertical eddy diffusion (which is the only transport in this pseudo 2-D model) cannot explain the observed behavior of the composition of Titan's low stratosphere, despite the realistic UV field. We are developing a real 2-D photochemical model, including the dynamics of the low atmosphere as modeled by *Hourdin et al.* [1995]. The simulated meridional winds form pole-to-pole Hadley cells at solstice, with subsidence in the winter hemisphere. This dynamical transport of species could help in building up the observed accumulations. This 2-D model has given very encouraging preliminary results [*Lebonnois et al.,* 1999].

6. Conclusion

This work on latitudinal diurnal averages of the actinic flux in a deep atmosphere confirms that for 1-D simulations, using a mean incident angle can avoid integration over the day. However, using $< \theta > = 30°$ for the annual average at the equator does not seem to be the best choice in Titan's case, $< \theta > = 50°$ being a better approximation. Nevertheless, the 3-D radiative transfer Monte Carlo code presented here allows us to confirm the importance of the use of 3-D calculations to evaluate the photolysis coefficients for which the contributions before sunrise or after sunset, neglected in 1-D models, can significantly contribute to the mean solar flux (e.g., high-latitude winter conditions). This major difference between 1-D and 3-D diurnal averages of the actinic fluxes is critical for the modeling of season-dependent photochemistry over Titan's high latitudes. We also show from 3-D results and from an adapted photochemical model that the explanation given by *Yung* [1987] for the enhancement of nitriles at high latitudes coming out of winter is not sufficient, despite the effects of latitude and season on the photolysis rates. It will be necessary to investigate a 2-D photochemical model including dynamics of the low atmosphere to understand Voyager observations [*Coustenis et al.,* 1995] and to prepare for the interpretation of Cassini-Huygens results.

Acknowledgment. This work was supported by the Programme National de Planétologie of the Institut National des Sciences de l'Univers (CNRS).

References

Cogley, A. C., and W. J. Borucki, Exponential approximation for daily average solar heating or photolysis, *J. Atmos. Sci., 33,* 1347-1356, 1976.

Coustenis, A., and B. Bézard, Titan's atmosphere from Voyager infrared observations, IV, Latitudinal variations of temperature and composition, *Icarus, 115,* 126-140, 1995.

Coustenis, A., B. Bézard, and D. Gautier, Titan's atmosphere from Voyager infrared observations, I, The gas composition of Titan's equatorial region, *Icarus, 80,* 54-76, 1989.

Hourdin, F., O. Talagrand, R. Sadourny, R. Courtin, D. Gautier, and C. P. McKay, Numerical simulation of the general circulation of the atmosphere of Titan, *Icarus, 117,* 358-374, 1995.

Lara, L. M., E. Lellouch, J. J. López-Moreno, and R. Rodrigo, Vertical distribution of Titan's atmospheric neutral constituents, *J. Geophys. Res., 101*(E10), 23,261-23,283, 1996.

Lebonnois, S., D. Toublanc, and F. Hourdin, Modeling the latitudinal variations in Titan's atmospheric composition with a 2-D photochemical model, *Bull. Am. Astron. Soc., 31*(4), in press, 1999.

Michelangeli, D.V., M. Allen, Y. L. Yung, R.-L. Shia, D. Crisp, and J. Eluszkiewicz, Enhancement of atmospheric radiation by an aerosol layer, *J. Geophys. Res., 97*(D1), 865-874, 1992.

Rannou, P., M. Cabane, E. Chassefière, R. Botet, C. P. McKay, and R. Courtin, Titan's geometric albedo: Role of the fractal sturcture of the aerosols, *Icarus, 118,* 355-372, 1995.

Sagan, C., and W. R. Thompson, Production and condensation of organic gases in the atmosphere of Titan, *Icarus, 59,* 113-161, 1984.

Toublanc, D., Henyey-Greenstein and Mie phase functions in Monte Carlo radiative transfer computations, *Appl. Opt., 35*(18), 3270-3274, 1996.

Toublanc, D., J. P. Parisot, J. Brillet, D. Gautier, F. Raulin, and C. P. McKay, Photochemical modeling of Titan's atmosphere, *Icarus, 113,* 2-26, 1995.

Yung, Y. L., An update of nitrile photochemistry on Titan, *Icarus, 72,* 468-472, 1987.

Yung, Y. L., M. Allen, and J. P. Pinto, Photochemistry of the atmosphere of Titan: Comparison between model and observations, *Astrophys. J. Suppl. Ser., 55,* 465-506, 1984.

S. Lebonnois and D. Toublanc, Centre d'Etude Spatiale des Rayonnements, 9 avenue du Colonel Roche, BP 4346, F-31028 Toulouse cedex 04, France. (lebonnois@cesr.fr; toublanc@cesr.fr)

(Received April 1, 1999; revised June 21, 1999;
accepted June 23, 1999.)